LETTER

doi:10.1038/nature09879

Recapitulation of premature ageing with iPSCs from Hutchinson–Gilford progeria syndrome

Guang-Hui Liu[1], Basam Z. Barkho[1], Sergio Ruiz[1], Dinh Diep[2], Jing Qu[1], Sheng-Lian Yang[1], Athanasia D. Panopoulos[1], Keiichiro Suzuki[1], Leo Kurian[1], Christopher Walsh[1], James Thompson[3], Stephanie Boue[4], Ho Lim Fung[2], Ignacio Sancho-Martinez[1], Kun Zhang[2], John Yates III[3] & Juan Carlos Izpisua Belmonte[1,4]

Hutchinson–Gilford progeria syndrome (HGPS) is a rare and fatal human premature ageing disease[1–5], characterized by premature arteriosclerosis and degeneration of vascular smooth muscle cells (SMCs)[6–8]. HGPS is caused by a single point mutation in the lamin A (*LMNA*) gene, resulting in the generation of progerin, a truncated splicing mutant of lamin A. Accumulation of progerin leads to various ageing-associated nuclear defects including disorganization of nuclear lamina and loss of heterochromatin[9–12]. Here we report the generation of induced pluripotent stem cells (iPSCs) from fibroblasts obtained from patients with HGPS. HGPS-iPSCs show absence of progerin, and more importantly, lack the nuclear envelope and epigenetic alterations normally associated with premature ageing. Upon differentiation of HGPS-iPSCs, progerin and its ageing-associated phenotypic consequences are restored. Specifically, directed differentiation of HGPS-iPSCs to SMCs leads to the appearance of premature senescence phenotypes associated with vascular ageing. Additionally, our studies identify DNA-dependent protein kinase catalytic subunit (DNAPKcs, also known as PRKDC) as a downstream target of progerin. The absence of nuclear DNAPK holoenzyme correlates with premature as well as physiological ageing. Because progerin also accumulates during physiological ageing[6,12,13], our results provide an *in vitro* iPSC-based model to study the pathogenesis of human premature and physiological vascular ageing.

Three HGPS primary fibroblast lines, originally isolated from patients with the classical *LMNA* mutation (Gly608Gly), were transduced with retroviruses encoding OCT4, SOX2, KLF4, c-MYC and green fluorescent protein (GFP). NANOG-positive colonies were effectively obtained when using early passage, but not late passage (>25), HGPS fibroblasts (Supplementary Fig. 1a). We focused on iPSC lines of a well characterized HGPS fibroblast line, AG01972 (refs 9–12). Compared to normal fibroblasts, HGPS fibroblasts (AG01972) showed abnormal nuclear morphology, reduced expression of the lamina components lamin B1 and LAP2β (also known as TMPO), loss of heterochromatin markers H3K9me3, HP1α (also known as CBX5) and HDAC1, and reduced expression of nuclear proliferation marker Ki67 (also known as MKI67; Fig. 1a and Supplementary Fig. 2). From HGPS fibroblasts, we derived six iPSC lines. In addition, we generated control iPSC lines from wild-type fibroblasts (BJ and IMR-90 cell lines). Control and HGPS iPSC lines demonstrated pluripotent gene expression, demethylation of the OCT4 promoter and transgene silencing (Fig. 1b and Supplementary Figs 1, 3 and 4a, and data not shown). They were maintained for more than 50 passages without a loss of pluripotency or the acquisition of detectable morphological or growth abnormalities. The pluripotency of each iPSC line was assessed by differentiation into the three embryonic germ layers *in vitro*, using embryoid body (EB) formation, and/or *in vivo*, by teratoma formation (Supplementary Fig. 5a–d). Out of these lines, we focused primarily on HGPS-iPSC#4 and BJ-iPSC#3 for our studies (hereafter referred to as HGPS-iPSC or BJ-iPSC). Both BJ-iPSCs and HGPS-iPSCs were able to differentiate towards specialized mesoderm-derivatives such as smooth muscle cells (SMC), endothelial cells (Supplementary Fig. 6a), or beating cardiomyocytes (Supplementary Movies 1 and 2). Moreover, all analysed iPSC lines showed normal chromosomal integrity (Supplementary Fig. 5e). Finally, *LMNA* sequencing confirmed the presence of the classical mutation in HGPS-iPSCs (Supplementary Fig. 5f). Altogether, these data indicate that the somatic cells from HGPS patients, despite their significant premature senescence phenotypes and nuclear defects, have been properly reprogrammed and can be effectively maintained in a pluripotent state.

Lamin A/C protein is expressed in differentiated somatic cells but is absent in embryonic stem cells (ESCs)[11,14]. Therefore, we next examined the expression of lamin A/C in the generated iPSC lines. As shown in Fig. 2a, lamin A/C expression is significantly downregulated in iPSCs, compared to their parental fibroblasts, whereas lamin B1 transcripts were upregulated. Although progerin should follow a similar pattern of expression as observed for lamin A/C, *LMNA* expression is independent

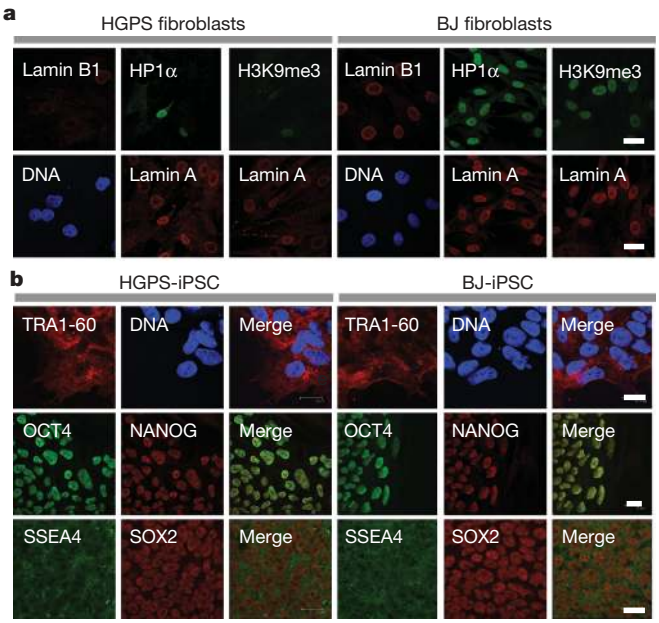

Figure 1 | Generation of iPSCs from HGPS fibroblasts. **a**, Immunofluorescence analysis performed on HGPS (left) and BJ (right) fibroblasts at passage 17 with the indicated antibodies. **b**, Immunofluorescence analysis of the indicated pluripotent markers in HGPS-iPSCs (left) and BJ-iPSCs (right). Nuclei were visualized with Hoechst stain (blue). Scale bar, 20 μm.

[1]Gene Expression Laboratory, Salk Institute for Biological Studies, 10010 North Torrey Pines Road, La Jolla, California 92037, USA. [2]Department of Bioengineering, University of California at San Diego, La Jolla, California 92093, USA. [3]Department of Cell Biology, Scripps Research Institute, La Jolla, California 92037, USA. [4]Center for Regenerative Medicine in Barcelona, Dr. Aiguader 88, 08003 Barcelona, Spain.

of promoter methylation status (Supplementary Fig. 4b)[15]. Indeed, a complete loss of progerin mRNA in HGPS-iPSCs was observed (Fig. 2a). Furthermore, expression of lamin A/C and progerin proteins was practically undetectable (Fig. 2b and Supplementary Fig. 4c).

Because HGPS-iPSCs did not express progerin, we examined whether the nuclear abnormalities observed in HGPS fibroblasts would also be absent at the pluripotent stage. Our results indicate that all of the epigenetic, nuclear lamina and proliferation parameters analysed in HGPS-iPSCs are indistinguishable from BJ-iPSCs (Fig. 2b, c and Supplementary Figs 3 and 7). In addition, the nuclei of HGPS-iPSCs displayed the characteristic wrinkles and lobes observed in hESCs and iPSCs (Supplementary Fig. 8), indicative of a reprogramming of the nuclear envelope components. As the nuclear envelope associates with and regulates heterochromatin[11,16], we next examined genome-wide CpG methylation in HGPS fibroblasts, BJ fibroblasts, HGPS-iPSCs, BJ-iPSCs, and H9 hESCs. Using bisulphite padlock probes and Illumina sequencing, we captured and quantified the methylation level of an average of 95,932 CpG sites within a set of 16,206 well-annotated differentially methylated regions (DMRs)[17] per cell line (Supplementary Table 1). The correlation coefficient of the global methylation levels between the pluripotent lines (BJ-iPSCs, HGPS-iPSCs and H9 hESCs) and the corresponding fibroblasts indicated that the generated pluripotent lines are much more closely related to each other and to hESCs than the two fibroblast lines (Fig. 2d). Interestingly, 586 autosome genes were found to be associated with regions that showed methylation differences between HGPS and BJ fibroblasts (Supplementary Table 2 and Supplementary Fig. 9a). Furthermore, based on DAVID[18,19] analysis, we found that these genes were enriched for 21 Gene Ontology terms, most of which were related to development and transcriptional regulation (Supplementary Fig. 9a). In contrast, methylation differences between HGPS-iPSCs and BJ-iPSCs were only found for 33 autosome genes (Supplementary Table 3), which showed no significant functional enrichment. Therefore, the presence of progerin in HGPS fibroblasts seems to lead to major epigenomic changes in various pathways. These changes were no longer present in HGPS-iPSCs, coinciding with the down-regulation of progerin. Finally, genome-wide mRNA profiling demonstrated that HGPS-iPSCs and BJ-iPSCs are closely related together with H9 hESCs, and different from their parental fibroblasts (Supplementary Fig. 9b–d). These results demonstrate the complete resetting of the nuclear architecture, epigenome and global gene expression in HGPS cells after being reprogrammed to pluripotency.

To test whether the expression of progerin could be re-activated, we first subjected HGPS-iPSCs to *in vitro* differentiation via EB formation. Progerin mRNA was selectively induced in differentiated HGPS-iPSCs, but not in differentiated BJ-iPSCs (Supplementary Fig. 10a). In contrast, lamin A was upregulated in both differentiated HGPS-iPSCs and differentiated BJ-iPSCs (Supplementary Fig. 10a). This reversible suppression of progerin expression by reprogramming, and subsequent reactivation upon differentiation, provides a unique model system to study human premature ageing pathologies. Progerin is known to accumulate mainly in arterial SMCs of HGPS patients, and vascular SMC degeneration is one of the characteristics of HGPS-associated arteriosclerosis[6,7,20]. In fact, vascular SMC senescence has been involved in the advanced arteriosclerosis of normal populations[7,21,22]. Therefore, we next asked whether SMCs differentiated from HGPS-iPSCs exhibit premature senescence phenotypes. Using a directed differentiation protocol, we obtained SMC populations from HGPS-iPSCs and BJ-iPSCs, the majority of which expressed characteristic SMC markers such as smooth muscle actin (SMA) and calponin (Supplementary Fig. 6a). Immunoblotting and PCR with reverse transcription (RT–PCR) analyses confirmed the expression of progerin in HGPS-iPSC, but not BJ-iPSC-derived SMCs (hereafter referred to as 'HGPS-SMC' and 'BJ-SMC', Supplementary Fig. 6b, c). To model SMC senescence *in vitro*, the differentiated SMCs were serially passaged in culture. As shown in Fig. 3a–c and Supplementary Fig. 10b, an increasing frequency of misshapen nuclei and a loss of the heterochromatin mark H3K9me3

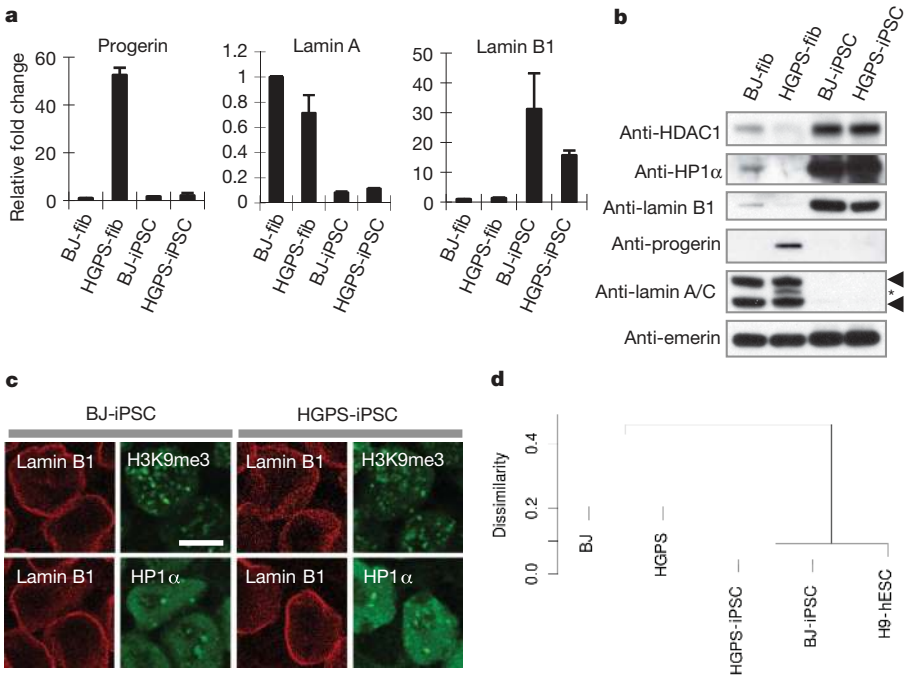

Figure 2 | HGPS-associated nuclear defects are reset in HGPS-iPSCs. a, RT–PCR analysis of progerin, lamin A and lamin B1 in the specific cell lines ($n = 3$). BJ- and HGPS-fib, BJ and HGPS fibroblasts. **b**, Immunoblotting analysis of the indicated proteins. Emerin was used as loading control. Asterisk denotes progerin (Δ50 lamin A). Arrowheads denote lamin A (top) and lamin C (bottom). **c**, Immunofluorescence analysis performed on BJ-iPSCs and HGPS-iPSCs for detection of the indicated proteins. Scale bar, 10 μm. **d**, Hierarchical clustering of genome-wide DNA methylation profiles.

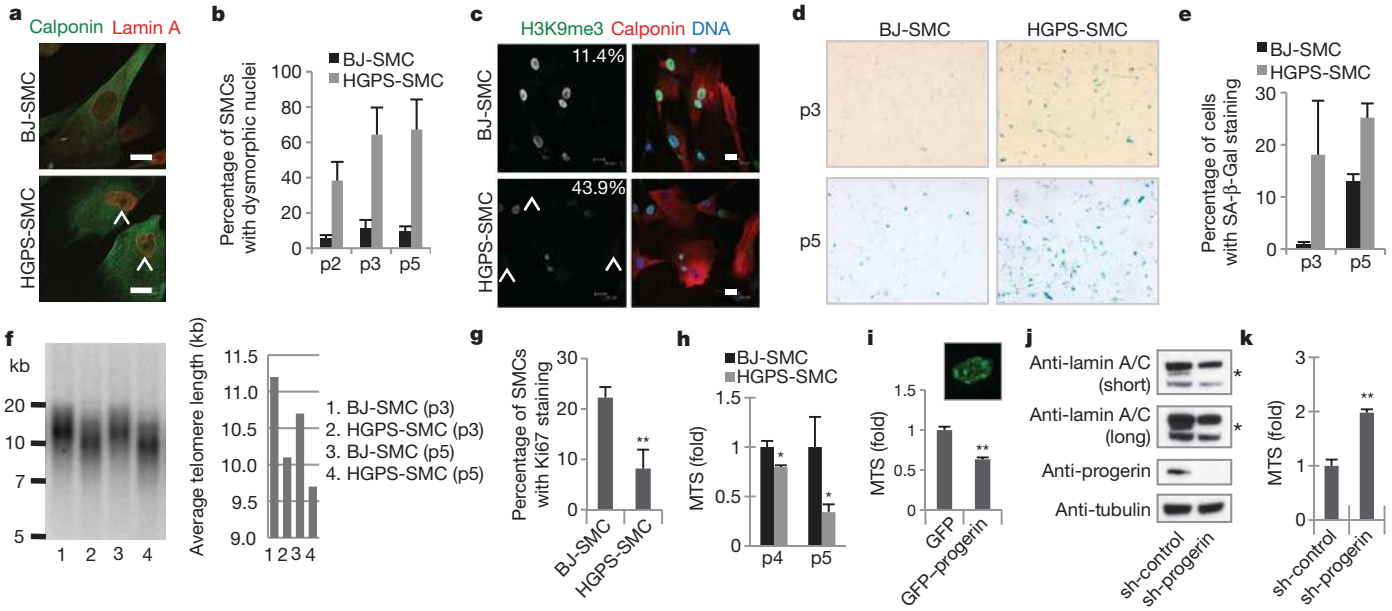

Figure 3 | SMCs expressing progerin show nuclear defects and accelerated senescence. **a**, Immunostaining of calponin and lamin A in iPSC-derived SMCs (p5). Arrowheads denote dysmorphic nuclei. Scale bar, 20 μm. **b**, Percentage of calponin-positive cells showing dysmorphic nuclei, ($n = 3$, $P < 0.001$). p2, p3 and p5, passage 2, 3 and 5, respectively. **c**, Immunostaining of H3K9me3 and calponin in iPSC-derived SMCs (p5). Nuclei were visualized with Hoechst stain (blue). Arrowheads denote decreased nuclear H3K9me3 (percentage in corner). Scale bar, 20 μm. **d**, **e**, Senescence-associated (SA)-β-Gal staining of iPSC-derived SMCs, $P < 0.05$. **f**, Southern blot analysis of SMCs showing telomere length (left). Quantified average of telomere length (right, $n = 2$). **g**, Percentage of Ki67-positive cells in iPSC-derived SMCs (calponin-positive, p3), $^{**}P < 0.01$. **h**, **i**, Cell proliferation analysis of iPSC-derived SMCs ($n = 3$), $^{*}P < 0.05$ (**h**) or primary vascular SMCs (overexpressing GFP or GFP–progerin, $n = 3$), $^{**}P < 0.01$ (**i**). Typical GFP–progerin-positive nucleus showing abnormal morphology (inset). **j**, Immunoblotting of the indicated proteins in shRNA-modified HGPS-iPSCs after 21 days of EB-mediated differentiation. Asterisks denote progerin (Δ50 lamin A). **k**, Cell proliferation analysis of the SMCs derived from shRNA-modified HGPS-iPSCs (p2, $n = 3$), $^{**}P < 0.01$.

were specifically observed in HGPS-SMCs after serial passaging. HGPS-SMCs at later passages (that is, passage 5) showed the typical characteristics of premature senescence, including increased senescence-associated-β-galactosidase (SA-β-Gal) staining (Fig. 3d, e and Supplementary Fig. 10c), reduced telomere length (Fig. 3f), a reduced number of Ki67-positive cells (Fig. 3g and Supplementary Fig. 10d), and compromised cell proliferation (Fig. 3h and Supplementary Fig. 10e). We also found a selective upregulation of senescence-related transcripts in HGPS-SMCs (Supplementary Fig. 10f). To test whether the observed HGPS-related cell phenotypes were specific to SMCs, we differentiated HGPS-iPSCs into fibroblasts and measured progerin-associated parameters. Progerin expression in HGPS-iPSC-derived fibroblasts was detectable as early as passage 5 (Supplementary Fig. 11a). However, we were unable to detect a loss of lamina or heterochromatin markers before passage 10 (Supplementary Fig. 11b, c). Nonetheless, these defects were present specifically in HGPS-iPSC-derived fibroblasts, in contrast to control iPSC-derived fibroblasts analysed at similar passage (data not shown). Thus, even though direct comparison of SMCs and fibroblasts is not possible due to their different culture conditions, our observations demonstrate that mesoderm lineages derived from HGPS-iPSCs display a characteristic HGPS phenotype.

We next investigated whether progerin accumulation is the direct cause of the accelerated cell senescence observed in HGPS-SMCs. To this end, we induced ectopic expression of progerin in human primary vascular SMCs. We found that introduction of progerin in wild-type SMCs resulted in compromised cell proliferation and nuclear defects, as we had observed in HGPS-SMCs (Fig. 3i and Supplementary Fig. 12). As a complementary approach, we transduced HGPS-iPSCs with a lentiviral vector expressing a progerin-specific short hairpin RNA (shRNA)[23]. The modified iPSCs showed normal karyotypes as well as normal expression of lamina/epigenetic and pluripotent markers (Supplementary Fig. 13a, b). After EB-based differentiation, both the mRNA and protein levels of progerin, but not those of lamin A, were substantially downregulated in the progerin-shRNA 'corrected' HGPS-iPSCs compared to control cells (Fig. 3j and Supplementary Fig. 13c, d). We next differentiated these 'progerin-free' HGPS-iPSCs into SMCs (Supplementary Fig. 14a). A marked improvement in the proliferation capability, as well as a downregulation of senescence-related transcripts, was found in the SMCs differentiated from the corrected HGPS-iPSCs (Fig. 3k and Supplementary Fig. 14b, c). Furthermore, transduction of progerin shRNA into early passage HGPS-iPSC-derived fibroblasts resulted in a clear restoration of nuclear morphology and heterochromatin markers after extended culture (Supplementary Fig. 15). Taken together, these data identify progerin as the key factor underlying the premature senescence phenotypes of HGPS-iPSC-derived cells.

Because phenotypic characteristics of premature ageing were able to be recapitulated by directed differentiation of the HGPS-iPSCs, we next investigated whether this model could serve to identify novel senescence-related markers. By using a sensitive MudPIT proteomic approach[24,25], we identified DNA-dependent protein kinase catalytic subunit (DNAPKcs) as a hitherto unknown binding partner of progerin (Supplementary Table 4). DNAPK holoenzyme, comprising DNAPKcs and its regulatory subunits Ku70/Ku80 (also known as XRCC6 and XRCC5, respectively), is involved in various ageing-related cellular events[26,27], and DNAPKcs or Ku70/Ku80-deficient mice exhibit accelerated ageing[27,28]. To further confirm the association of progerin with DNAPKcs, we performed co-immunoprecipitation experiments. As shown in Fig. 4a, ectopically expressed progerin associated tightly with endogenous DNAPKcs. In contrast, lamin A showed weak interaction with DNAPKcs, whereas both progerin and lamin A exhibited similar binding to lamin B1. Neither progerin nor lamin A co-immunoprecipitated with endogenous WRN protein. Since most of

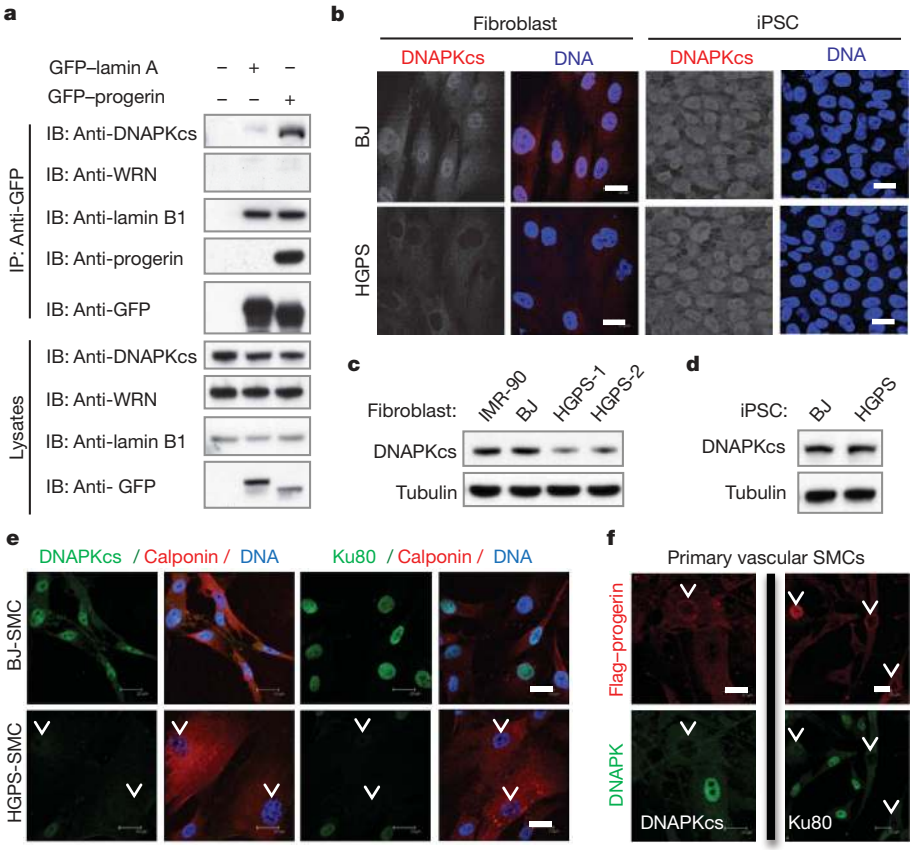

Figure 4 | Decreased expression of DNAPK holoenzyme correlates with premature cell ageing. **a**, Extracts from BJ fibroblasts expressing GFP, GFP–lamin A, or GFP–progerin, were immunoprecipitated (IP) with a GFP antibody and examined by immunoblotting analysis (IB). **b**, DNAPKcs staining in the indicated cell lines. **c**, **d**, Immunoblot analysis of DNAPKcs expression. **e**, **f**, Immunostaining of the indicated proteins in iPSCs-derived SMCs (**e**) or primary vascular SMCs overexpressing progerin (**f**). Arrowheads denote decreased DNAPKcs or Ku80. Nuclei were visualized with Hoechst stain (blue). Scale bar, 20 μm.

the nuclear proteins in complex with lamin A are destabilized in HGPS cells[9,29], we analysed the status of DNAPKcs in primary HGPS fibroblasts. We observed decreased nuclear DNAPKcs in HGPS fibroblasts when compared to normal fibroblasts (Fig. 4b, c). In addition, the regulatory subunits Ku70/Ku80 were also downregulated in HGPS fibroblasts (Supplementary Fig. 16a). Interestingly, we detected a complete restoration of DNAPKcs/Ku70/Ku80 expression in HGPS-iPSCs (Fig. 4b, d and Supplementary Figs 3 and 16b), although a deficiency in the expression of these proteins reappeared after differentiation into SMCs (Fig. 4e). These observations indicate that the downregulation of DNAPKcs in HGPS cells is dependent on the accumulation of progerin in differentiated cells. In fact, ectopic expression of progerin in primary vascular SMCs diminished DNAPKcs/Ku80 protein expression (Fig. 4f and Supplementary Fig. 17). We next tested whether inactivation of DNAPKcs could partially contribute to some of the phenotypes observed in HGPS-SMCs. We found that knockdown of DNAPKcs reduced the proliferation of primary vascular SMCs (Supplementary Fig. 18a). Finally, we extended our results and found that progressive loss of DNAPKcs/Ku70/Ku80 also occurs in fibroblasts isolated from normally ageing individuals (Supplementary Fig. 18b). Overall, our data indicate that deficiency of the DNAPK holoenzyme may constitute a novel marker for premature as well as physiological ageing.

In summary, our results not only highlight the plasticity of the lamina-epigenetics axis, but also point to the fact that the altered structure of the nuclear envelope, as well as the epigenetic modifications that accumulate during physiological ageing[12] or under specific disease conditions[1,11], can be restored to normalcy by reprogramming (Supplementary Fig. 19). The gradual onset and complexity of ageing has impeded progress in understanding the pathogenesis of ageing-related cardiovascular disorders. Recently, striking similarities between normal ageing-associated and HGPS-associated arteriosclerosis have been reported[6,16]. Indeed, the levels of progerin increase gradually during physiological ageing[6]. Our study provides the first evidence that, in a progerin-dependent manner, HGPS-iPSC-derived SMCs reach senescence-related phenotypes earlier than their normal counterparts. The iPSC-based accelerated ageing model presented here and in ref. 30 may provide an avenue to model and study the pathogenesis of human ageing-related vascular diseases as well as various human laminopathies[1].

METHODS SUMMARY

iPSCs were generated from human fibroblasts with retroviruses encoding OCT4/SOX2/KLF4/c-MYC/GFP, and grown on MEF feeder cells or Matrigel. SMCs were differentiated from iPSCs-derived $CD34^+$ progenitor cells following an OP9-based protocol.

Full Methods and any associated references are available in the online version of the paper at www.nature.com/nature.

Received 24 September 2010; accepted 1 February 2011.
Published online 23 February 2011.

1. Worman, H. J., Ostlund, C. & Wang, Y. Diseases of the nuclear envelope. *Cold Spring Harb. Perspect. Biol.* **2,** a000760 (2010).
2. Burtner, C. R. & Kennedy, B. K. Progeria syndromes and ageing: what is the connection? *Nature Rev. Mol. Cell Biol.* **11,** 567–578 (2010).
3. Kudlow, B. A., Kennedy, B. K. & Monnat, R. J. Jr. Werner and Hutchinson–Gilford progeria syndromes: mechanistic basis of human progeroid diseases. *Nature Rev. Mol. Cell Biol.* **8,** 394–404 (2007).
4. Merideth, M. A. *et al.* Phenotype and course of Hutchinson–Gilford progeria syndrome. *N. Engl. J. Med.* **358,** 592–604 (2008).

5. Davies, B. S., Fong, L. G., Yang, S. H., Coffinier, C. & Young, S. G. The posttranslational processing of prelamin A and disease. *Annu. Rev. Genomics Hum. Genet.* **10,** 153–174 (2009).
6. Olive, M. *et al.* Cardiovascular pathology in Hutchinson-Gilford progeria: correlation with the vascular pathology of aging. *Arterioscler. Thromb. Vasc. Biol.* doi:10.1161/ATVBAHA.110.209460 (26 August 2010).
7. Ragnauth, C. D. *et al.* Prelamin A acts to accelerate smooth muscle cell senescence and is a novel biomarker of human vascular aging. *Circulation* **121,** 2200–2210 (2010).
8. Varga, R. *et al.* Progressive vascular smooth muscle cell defects in a mouse model of Hutchinson–Gilford progeria syndrome. *Proc. Natl Acad. Sci. USA* **103,** 3250–3255 (2006).
9. Pegoraro, G. *et al.* Ageing-related chromatin defects through loss of the NURD complex. *Nature Cell Biol.* **11,** 1261–1267 (2009).
10. Scaffidi, P. & Misteli, T. Reversal of the cellular phenotype in the premature aging disease Hutchinson-Gilford progeria syndrome. *Nature Med.* **11,** 440–445 (2005).
11. Dechat, T. *et al.* Nuclear lamins: major factors in the structural organization and function of the nucleus and chromatin. *Genes Dev.* **22,** 832–853 (2008).
12. Scaffidi, P. & Misteli, T. Lamin A-dependent nuclear defects in human aging. *Science* **312,** 1059–1063 (2006).
13. McClintock, D. *et al.* The mutant form of lamin A that causes Hutchinson-Gilford progeria is a biomarker of cellular aging in human skin. *PLoS ONE* **2,** e1269 (2007).
14. Constantinescu, D., Gray, H. L., Sammak, P. J., Schatten, G. P. & Csoka, A. B. Lamin A/C expression is a marker of mouse and human embryonic stem cell differentiation. *Stem Cells* **24,** 177–185 (2006).
15. Freberg, C. T., Dahl, J. A., Timoskainen, S. & Collas, P. Epigenetic reprogramming of OCT4 and NANOG regulatory regions by embryonal carcinoma cell extract. *Mol. Biol. Cell* **18,** 1543–1553 (2007).
16. Peric-Hupkes, D. *et al.* Molecular maps of the reorganization of genome-nuclear lamina interactions during differentiation. *Mol. Cell* **38,** 603–613 (2010).
17. Irizarry, R. A. *et al.* The human colon cancer methylome shows similar hypo- and hypermethylation at conserved tissue-specific CpG island shores. *Nature Genet.* **41,** 178–186 (2009).
18. Huang, W., Sherman, B. T. & Lempicki, R. A. Systematic and integrative analysis of large gene lists using DAVID bioinformatics resources. *Nature Protocols* **4,** 44–57 (2009).
19. Dennis, G. *et al.* DAVID: database for annotation, visualization, and integrated discovery. *Genome Biol.* **4,** R60 (2003).
20. McClintock, D., Gordon, L. B. & Djabali, K. Hutchinson–Gilford progeria mutant lamin A primarily targets human vascular cells as detected by an anti-Lamin A G608G antibody. *Proc. Natl Acad. Sci. USA* **103,** 2154–2159 (2006).
21. Gorenne, I., Kavurma, M., Scott, S. & Bennett, M. Vascular smooth muscle cell senescence in atherosclerosis. *Cardiovasc. Res.* **72,** 9–17 (2006).
22. Minamino, T. & Komuro, I. Vascular cell senescence: contribution to atherosclerosis. *Circ. Res.* **100,** 15–26 (2007).
23. Huang, S. *et al.* Correction of cellular phenotypes of Hutchinson-Gilford progeria cells by RNA interference. *Hum. Genet.* **118,** 444–450 (2005).
24. Liu, G. H. *et al.* Regulation of myoblast differentiation by the nuclear envelope protein NET39. *Mol. Cell. Biol.* **29,** 5800–5812 (2009).
25. Washburn, M. P., Wolters, D. & Yates, J. R., III. Large-scale analysis of the yeast proteome by multidimensional protein identification technology. *Nature Biotechnol.* **19,** 242–247 (2001).
26. Ruis, B. L., Fattah, K. R. & Hendrickson, E. A. The catalytic subunit of DNA-dependent protein kinase regulates proliferation, telomere length, and genomic stability in human somatic cells. *Mol. Cell. Biol.* **28,** 6182–6195 (2008).
27. Li, H., Vogel, H., Holcomb, V. B., Gu, Y. & Hasty, P. Deletion of Ku70, Ku80, or both causes early aging without substantially increased cancer. *Mol. Cell. Biol.* **27,** 8205–8214 (2007).
28. Espejel, S. *et al.* Shorter telomeres, accelerated ageing and increased lymphoma in DNA-PKcs-deficient mice. *EMBO Rep.* **5,** 503–509 (2004).
29. Han, X. *et al.* Tethering by lamin A stabilizes and targets the ING1 tumour suppressor. *Nature Cell Biol.* **10,** 1333–1340 (2008).
30. Zhang, J. *et al.* A human iPSC model of Hutchinson Gilford progeria reveals vascular smooth muscle and mesenchymal stem cell defects. *Cell Stem Cell* **8,** 31–45 (2011).

Supplementary Information is linked to the online version of the paper at www.nature.com/nature.

Acknowledgements We thank L. Comai for providing experimental material, M. Hetzer, J. Karlseder, J.-F. Deleuze, M. J. Barrero, C. Rodriguez Esteban and L. Gerace for helpful discussions, M. Marti for teratoma analysis, M. C. Llach for karyotyping, T. Berggren, M. Lutz, I. Dubova, S. Stewart, R. Dev, M. Li, L. Laricchia-Robbio, A. M. Goebl and J. Kim for technical help, and M. Schwarz for administrative help. G.-H.L. and L.K. were partially supported by a CIRM grant (TG2-01158), J.Q. was partially supported by an AFAR/Ellison Medical Foundation postdoctoral fellowship; A.D.P. was partially supported by a NIH training grant T32 CA009370. This study was supported by grants from NIH R01-DA025779 (K.Z.), and NIH P41 RR011823 (J.Y.); the G. Harold and Leila Y. Mathers Charitable Foundation, Sanofi-Aventis, Ellison Medical Foundation, MICINN and Fundacion Cellex (JCIB).

Author Contributions G.-H.L. and J.C.I.B. conceived the experiments; G.-H.L., B.Z.B., S.R., D.D., J.Q., S.-L.Y., A.D.P., K.S., L.K., C.W., J.T. and H.L.F. performed the experiments and analysed the data; S.B., I.S.-M., K.Z., J.Y. and J.C.I.B. analysed the data; G.-H.L., S.R., B.Z.B., A.D.P., K.Z. and J.C.I.B. wrote the manuscript.

Author Information Microarray data have been deposited in NCBI-GEO under the accession number GSE24487. Reprints and permissions information is available at www.nature.com/reprints. The authors declare no competing financial interests. Readers are welcome to comment on the online version of this article at www.nature.com/nature. Correspondence and requests for materials should be addressed to J.C.I.B. (belmonte@salk.edu, izpisua@cmrb.eu).

METHODS

Cell culture. H9 hESCs (WiCell Research) and iPSCs were maintained on a layer of mitotically inactivated mouse embryonic fibroblasts (MEFs) in hESC medium: DMEM/F12 (Invitrogen) supplemented with 0.1 mM non-essential amino acids (Invitrogen), 1 mM GlutaMAX (Invitrogen), 20% Knockout Serum Replacement (Invitrogen), 55 μM β-mercaptoethanol (Invitrogen) and 10 ng ml^{-1} bFGF (Joint Protein Central). hESCs and iPSCs were also cultured in Matrigel (BD Biosciences) with mTeSR medium (Stem Cell Technologies). Human HGPS fibroblasts AG01972, AG11498, AG06297, and normal fibroblasts GM00038 (9 years), AG05247 (87 years), and AG09602 (92 years) were purchased from Coriell Cell Repository. BJ normal human fibroblasts (CRL-2522) were purchased from ATCC. All human fibroblasts were cultured at 37 °C in DMEM containing GlutaMAX, non-essential amino acids, sodium pyruvate, and 15% fetal bovine serum (FBS). Human aortic smooth muscle cells were purchased from Lonza and maintained in SmGM-2 medium (Lonza, Cat. # CC-3182).

Reagents. Antibodies were obtained from the following sources. Abcam: anti-NANOG (ab21624), anti-H3K9me3 (ab8898), anti-progerin (ab66587), anti-emerin (ab14208); anti-Ku70 (ab2172); Santa Cruz Biotechnology: anti-Oct-3/4 (sc-5279), anti-SOX2 (sc-17320), anti-HDAC1 (sc-7872), anti-DNAPKcs (sc-9051), anti-lamin A/C (sc-6215), anti-lamin A/C (sc-7293), anti-lamin B1 (sc-6217); Cell Signaling: anti-HP1α (2616); anti-Ku80 (2753); R&D systems: anti-Foxa2 (AF2400); Millipore: anti-TRA-1-60 (MAB4360) ; Sigma: anti-β-Tubulin III (T2200), anti-SMA(A5228), anti-Flag (M2), and anti-tubulin (T5168); Dako: anti-calponin (clone CALP); anti-endoglin (clone SN6h); BD Transduction Laboratories: anti-LAP2β (611000); MBL: agarose-conjugated anti-GFP.

Plasmids. The pMXs vector containing the human cDNAs for *OCT4*, *SOX2*, *KLF4* and *c-MYC* were purchased from Addgene (17217, 17218, 17219 and 17220, respectively). pBABE-puro-GFP-progerin and pBABE-puro-GFP-wt-lamin A were purchased from Addgene (17663 and 17662, respectively). Flag-progerin lentiviral vector was kindly provided by L. Comai[31]. For the generation of the shRNA expression vectors against progerin and DNAPKcs, corresponding oligonucleotides (see Supplementary Table 5) were cloned into a MluI–ClaI-cleaved pLVTHM plasmid (Addgene, 12247). All the constructs generated were subjected to DNA sequencing to confirm accurate shRNA target sequence.

Retrovirus and lentivirus production. For retrovirus production, 293T cells were transfected with the pMXs vectors carrying *OCT4*, *SOX2*, *c-MYC*, *KLF4* or *GFP* cDNAs, together with the packaging plasmids (pCMV-gag-pol-PA and pCMV-VSVg, provided by G. Pao, The Salk Institute) using Lipofectamine 2000 (Invitrogen). Retroviruses were collected 36–48 h after transfection, and filtered through a 0.45-μM filter. Lentiviruses were generated by co-transfecting the pLVTHM vector together with the packaging plasmids (psPAX2 and pMD2.G, from Addgene, 12260 and 12259 respectively) into 293T cells using Lipofectamine 2000 (Invitrogen). Lentiviruses were collected 36 h after transfection and concentrated by ultracentrifugation.

iPSCs generation. For the generation of human iPSCs, human fibroblasts were seeded in a 6-well plate and spin-infected with a mix of high-quality retroviruses encoding OCT4, SOX2, KLF4, c-MYC and GFP in the presence of 4 μg ml^{-1} polybrene. Three infections on consecutive days were performed. Six days after the first infection, fibroblasts were gently individualized with TrypLE (Invitrogen) and seeded onto fresh MEFs in the fibroblast culture medium. After 24 h, the medium was switched to hESC medium, and changed every 1–2 days depending on cell density. To establish the iPSC lines, colonies were manually picked and transferred onto MEF feeder cells for several passages before being transferred to Matrigel/mTeSR conditions.

Lentiviral infection of iPSCs. HGPS-iPSC#4 cell line cultured on Matrigel was treated with 10 μM ROCK inhibitor Y-27632 for 1 h and then individualized with TrypLE. Cells were infected in suspension with either the concentrated lentivirus pLVTHM or pLVTHM-shRNA-progerin in the presence of ROCK inhibitor and polybrene (4 μg ml^{-1}) for 1 h. Cells were centrifuged to remove the lentivirus and seeded back on fresh feeder MEFs in hESC media containing ROCK inhibitor. After growing for a few days, small colonies were manually passaged as a pool of colonies onto fresh MEFs to establish new iPSC lines. GFP expression was used as an indicator to determine successful integration of the lentiviruses.

Cell differentiation. For embryoid bodies (EBs) based differentiation, the iPSC colonies growing on MEFs were detached with dispase treatment, resuspended in DMEM/F12 medium supplemented with 0.1 mM non-essential amino acids, 0.5 mM L-glutamine, 10% FBS (Atlanta Biologicals), and 55 μM β-mercaptoethanol and cultured in low attachment 6-well plates for 4 days. The EBs were then plated on gelatin-coated plates and maintained for another 10–17 days. Differentiation of iPSCs into fibroblasts was performed as previously described[32]. Directed differentiation towards smooth muscle cells (SMCs) was performed essentially as previously described[33] with slight modifications. Irritated OP9 cells were plated at 1×10^5 cells per well onto gelatinized 6-well plates in OP9 growth medium. After the formation of confluent iPS cell cultures for 4 and 5 days, undifferentiated iPS cells were harvested by treatment with 1 mg ml^{-1} dispase and dispersed by scraping to maintain the cells in small clumps. Concurrently, iPS cultures growing under the same conditions were used to obtain single cell suspension for counting. The iPSCs were added to OP9 cultures at a density of 3×10^5 per 2 ml per well of a 6-well plate in half TeSR medium and half hESC media. iPSCs were allowed to recover for 1–2 days in hESC media. At day 0 of differentiation, the media was changed to Knockout DMEM supplemented with 10% FBS (HyClone), 10 mM β-mercaptoethanol, 1 mM L-glutamine, and 100 mM nonessential amino acids. The iPSC/OP9 co-cultures were incubated for up to 10 days at 37 °C in 5% CO2 conditions with medium change every other day. After 10 days of differentiation, the co-culture cells were harvested with TrypLE (Invitrogen) for single-cell suspension and labelled with CD34 microbeads kit (Miltenyi Biotech, Cat. #130-046-702). Following the manufacturer's protocol, cells were passed through MS separation column attached to a Midi-MACS separation unit (Miltenyi Biotech) to obtain a magnet-retained fraction of purified CD34$^+$ cells. Isolated CD34$^+$ cells were then plated in smooth muscle cell media (SmGM-2 BulletKit, Lonza, Cat. # CC-3182) and maintained at 37 °C in 5% CO_2 conditions with medium change every 2–3 days[34]. SMCs were passaged using TrypLE (diluted 1:4) for 3 min at 37 °C. To analyse early onset of senescence, cells were passaged at a ratio of 1:3 (~6,000–7,500 cells per cm^2) only when the cells reached confluence. To calculate population doublings, SMCs seeded at 3,500 cells per cm^2 were passaged once culture reached 85–90% confluence. Cell growth was measured at every passage by calculation of accumulated population doublings using the formula ($\log H - \log S$)/log2.0 where H = number of cells harvested, S = number of cells seeded on the first day of each passage.

Protein and mRNA analysis. Cells were lysed and subjected to immunoblotting analysis according to the previously described method[35]. Total RNA was extracted using TRIzol (Invitrogen) followed by cDNA synthesis using High capability RNA-to-cDNA Mater Mix (Invitrogen). Quantitative RT–PCR was performed using SYBR Green PCR Master Mix (Applied Biosystems). Primer sequences are listed in Supplementary Table 5.

Immunofluorescence microscopy. Cells were fixed with 4% formaldehyde in PBS at room temperature for 20–30 min. After fixation, cells were treated with 0.4% Triton X-100 in PBS for 5 min at room temperature. After blocked with 10% FBS in PBS for 30 min, cells were incubated at room temperature for 1 h or at 4 °C overnight with the primary antibody, followed by washing in PBS and incubation at room temperature for 1 h with the corresponding secondary antibody. Nuclei were stained with Hoechst 33342 (Invitrogen). Quantitative microscopy measurements were carried out as described previously[9]. Error bars represent standard deviations.

Immunohistochemical detection of NANOG. Cells were fixed with 4% formaldehyde in PBS at room temperature for 30 min, and permeabilized with 0.4% Triton-X100 in PBS for 10 min. Then the cells were incubated overnight with rabbit anti-human NANOG antibody in 1% BSA/PBS, followed by incubation with a secondary biotin-conjugated anti-rabbit antibody for 2 h. Finally, cells were incubated with streptavidin-HRP for 1 h (Vector), and NANOG-positive cells were visualized with a DAB substrate kit (Vector).

Teratoma analysis. To test pluripotency *in vivo*, NOD-SCID IL2Rgamma^{null} mice (Jackson laboratories) were injected with the indicated iPSC lines and teratoma formation assessed. Briefly, ~10^6 iPSCs in ~50 μl of hESC medium were injected into the testis or kidney capsule of anesthetized mice. Mice were monitored for teratoma formation and euthanized ~6–12 weeks after injection. Teratomas were harvested, processed and analysed by haematoxylin–eosin staining and immunostaining. All animal experiments were performed with approval of The Salk Institute Institutional Animal Care and Use Committee (IACUC).

Mutation validation. Primer sequences to amplify exon 11 of the *LMNA* gene are listed in Supplementary Table 5. PCR (final volume 50 μl) reactions using 3 ng genomic DNA templates, 100 nM of the forward and reverse primers with 25 μl Taq 2× Master Mix (NEB) was performed at 94 °C for 2 min, 34 cycles of 94 °C 30 s, 55.5 °C for 40 s, and 72 °C for 40 s, and finally 72 °C for 3 min. Products were purified with 0.9× volume of AMPure beads (Agencourt). Amplicons were sequenced by capillary Sanger sequencing (Genewiz). Results were visualized using an ABI Sequence Scanner.

Genome-wide DNA methylation analysis. Genomic DNA was extracted using ALLPrep DNA/RNA Mini kit (Qiagen). Bisulphite conversion and capture reaction was carried out on each sample (genomic DNA of fibroblasts, iPSCs, or hESCs). The detailed protocol for genomic DNA methylation has been described previously[36], and the detailed information for DNA methylation is presented in Supplementary Table 1.

Bisulphite sequencing of OCT4 and *LMNA* promoters. Bisulphite conversion was carried out using 2 μg of purified genomic DNA using the Zymo EZ-DNA Methylation Gold Kit (Zymo Research) following the manufacturer's instructions. PCR was set up using previously published primers[15]. Cycling was terminated at 35

cycles. PCR products were purified using 2% Size-Select E-gel (Invitrogen) and reamplified for 10 cycles using Phusion HF enzyme (NEB). PCR products were cloned using Zero-blunt PCR Cloning kit (Invitrogen) and heat transfected to TOP10 *Escherichia coli* competent cells (Invitrogen). Individual colonies were selected and sent for single pass sequencing.

DNA microarray and bioinformatics analysis. The GeneChip microarray processing was performed by the Functional Genomica Core in the Institute for Research in Biomedicine (Barcelona, Spain) according to the manufacturer's protocols (Affymetrix). The amplification and labelling were processed as indicated in Nugen protocol with 25 ng starting RNA. For each sample, 3.75 μg ssDNA were labelled and hybridized to the Affymetrix HG-U133 Plus 2.0 chips. Expression signals were scanned on an Affymetrix GeneChip Scanner (7G upgrade). The data extraction was done by the Affymetrix GCOS software v.1.4.

The statistical analysis of the data was performed using ArrayStar 3. Briefly, raw CEL files were imported together with gene annotation from NetAffix (from 11/13/2009) and after checking for top replication quality for each of the five pairs of samples ($R^2 > 0.99$), data was summarized at the gene level (20,765 genes) and the median was used for each gene and sample type. As both H9 hESCs and HGPS-iPSCs originate from female samples, and in order to remove any possible bias introduced by the X and Y chromosome-coded genes, we performed the same analysis with only autosome genes (19,884 genes). The result of the hierarchical clustering is very similar to the one using all genes and is shown in Supplementary Fig. 9b. In addition, a principal component analysis was performed on RMA-normalized probeset intensity values for autosomes using the prcomp function in R (http://www.r-project.org/) (the same figure including all genes gave highly similar results, data not shown). A figure illustrating the two first principal components is shown in Supplementary Fig. 9c. Differences between some of the samples is shown using scatter plot of RMA-normalized intensity values in Supplementary Fig. 9d.

Multidimensional protein identification technology (MudPIT) analysis of progerin-associated proteins. The immunoprecipitation for MudPIT assay was performed as previously described[24,25]. In brief, HEK293T cells were transfected with GFP–progerin or GFP and maintained in culture for 48 h. After cells were lysed, the GFP–progerin, GFP, and their associated proteins were immunoadsorbed to anti-GFP agarose. The immunoprecipitates were then eluted with 8 M urea in 100 mM Tris, pH 8.5. The samples were reduced by adding 0.3 μl of 1 M TCEP (for a final concentration of 5 mM TCEP) and incubated at room temperature. To alkylate, 1.2 μl of iodoacetamide (10 mM final concentration) was added and the samples were subsequently incubated at room temperature in the dark for 15 min. The addition of 180 μl of 100 mM Tris pH 8.5 diluted the solutions to 2 M urea. Calcium chloride (100 mM) was then added (2.4 μl) for a final concentration of 1 mM $CaCl_2$. Trypsin (0.5 μg μl^{-1}) was added in the amount of 7.0 μl. The resulting mixtures were then shaken for 18 h and incubated in the dark at 37 °C. To neutralize 13.5 μl of formic acid (90%) was added for a final concentration of 5% formic acid. The tubes were centrifuged for 30 min at 2 °C in a table-top centrifuge. Upon completion of the digestion, the proteins were pressure-loaded onto a fused silica capillary desalting column containing 3 cm of 5-μm strong cation exchange (SCX) followed by 3 cm of 5-μm C18 (reverse phase or RP material) packed into an undeactivated 250-μm i.d capillary. Using 1.5 ml of buffer A (95% water, 5% acetonitrile and 0.1% formic acid) the desalting columns were washed overnight. Following the desalting process, a 100-μm internal diameter capillary consisting of a 10-μm laser pulled tip packed with 10 cm 3-μm Aqua C18 material (Phenomenex) was attached to the filter union (desalting column–filter union–analytical column) and the entire split-column (desalting column–filter union–analytical column) was placed in line with an Agilent 1100 quaternary HPLC (Palo Alto, CA) and analysed using a modified 6-step separation, described previously[25]. The buffer solutions used were 5% acetonitrile/0.1% formic acid (buffer A), 80% acetonitrile/0.1% formic acid (buffer B), and 500 mM ammonium acetate/5% acetonitrile/0.1% formic acid (buffer C). Step 1 consisted of a 90 min gradient from 0–100% buffer B. Steps 2–5 had the following profile: 3 min of 100% buffer A, 2 min of X% buffer C, a 10 min gradient from 0–15% buffer B, and a 97 min gradient from 15–45% buffer B. The 2 min buffer C percentages (X) were 20, 40, 60, 80% respectively for the 6-step analysis. In the final step, the gradient contained: 3 min of 100% buffer A, 20 min of 100% buffer C, a 10 min gradient from 0–15% buffer B, and a 107 min gradient from 15–70% buffer B. As peptides eluted from the microcapillary column, they were electrosprayed directly into an LTQ 2-dimensional ion trap mass spectrometer (ThermoFinnigan) with the application of a distal 2.4 kV spray voltage. A cycle of one full-scan mass spectrum (400–1,400 m/z) followed by 8 data-dependent MS/MS spectra at a 35% normalized collision energy was repeated continuously throughout each step of the multidimensional separation. Application of mass spectrometer scan functions and HPLC solvent gradients were controlled by the Xcalibur data system.

As each step was executed, its spectra were recorded to a RAW file. This data was then converted into .ms2 format through the use of RawXtract (Version 1.9). From the .ms2 files, poor quality spectra were removed from the data set using an automated spectral quality assessment algorithm[37]. MS/MS spectra remaining after filtering were searched with the SEQUEST algorithm[38] against the NCBI RefSeq Human (04-23-2010) protein database concatenated to a decoy database in which the sequence for each entry in the original database was reversed[25,39]. All searches were parallelized and performed on a Beowulf computer cluster consisting of 100 1.2 GHz Athlon CPUs[40]. No enzyme specificity was considered for any search. SEQUEST results were assembled and filtered using the DTASelect (version 2.0) program. DTASelect 2.0 uses a linear discriminant analysis to dynamically set XCorr and DeltaCN thresholds for the entire data set to achieve a user-specified false positive rate. The false positive rates are estimated by the program from the number and quality of spectral matches to the decoy database. The hits detected uniquely in the GFP–progerin sample but not in GFP sample represent proteins that are specifically associated with progerin, by either direct or indirect interactions.

Co-immunoprecipitation. BJ human fibroblasts were transduced with retrovirus encoding GFP–progerin, GFP–lamin A or GFP, and maintained in culture for 72 h. For immunoprecipitation, cells were lysed in ice-cold lysis buffer (250 mM NaCl, 0.5% Triton X-100, 50 mM Tris, pH 7.5, 1 mM EGTA, 1 mM EDTA, 10% glycerol, and complete protease inhibitor cocktail (Roche Diagnostics)). Samples were briefly sonicated and immunoprecipitated by incubating with anti-GFP agarose. The immunoprecipitates were washed extensively in lysis buffer, eluted in SDS sample buffer, and subjected to immunoblotting.

Senescence-associated beta-galactosidase (SA-βgal) assay. SA-βgal assay were performed based on previously described methods[41].

Measurement of telomere length. Genomic DNA was isolated from 1×10^6 cells. The telomere-specific oligonucleotide probe (5′-TTAGGGTTAGGGTTAGGG TTAGGG-3′; ValueGene) was end-labelled using γ-^{32}P-ATP (MP Biomedicals) and T4 polynucleotide kinase (NEB). Two μg of genomic DNA for each sample was digested with AluI (NEB) and MboI (NEB) and subjected to Southern analysis with the telomere-specific probe. Mean telomere length was calculated from $\sum OD_i/(\sum OD_i/\sum MW_i)$. OD_i and MW_i are optical density and molecular weight at a given position i, respectively.

Cell proliferation assay. Cell proliferation was determined with CellTiter 96 AQ_{ueous} One Solution Cell Proliferation Assay (MTS (3-(4,5-dimethylthiazol-2-yl)-2,5-diphenyltetrazolium)), according to the protocol provided by the manufacturer (Promega).

Statistical analysis. Results are presented as mean ± s.d. Comparisons were performed with student's t-test or one-way anova. $P < 0.05$ was defined as statistically significant.

31. Candelario, J., Borrego, S., Reddy, S. & Comai, L. Accumulation of distinct prelamin A variants in human diploid fibroblasts differentially affects cell homeostasis. *Exp. Cell Res.* **317,** 319–329 (2011).
32. Hockemeyer, D. *et al.* A drug-inducible system for direct reprogramming of human somatic cells to pluripotency. *Cell Stem Cell* **3,** 346–353 (2008).
33. Vodyanik, M. A., Bork, J. A., Thomson, J. A. & Slukvin, I. I. Human embryonic stem cell-derived CD34+ cells: efficient production in the coculture with OP9 stromal cells and analysis of lymphohematopoietic potential. *Blood* **105,** 617–626 (2005).
34. Lu, S. J., Ivanova, Y., Feng, Q., Luo, C. & Lanza, R. Hemangioblasts from human embryonic stem cells generate multilayered blood vessels with functional smooth muscle cells. *Regen. Med.* **4,** 37–47 (2009).
35. Kawamura, T. *et al.* Linking the p53 tumour suppressor pathway to somatic cell reprogramming. *Nature* **460,** 1140–1144 (2009).
36. Deng, J. *et al.* Targeted bisulfite sequencing reveals changes in DNA methylation associated with nuclear reprogramming. *Nature Biotechnol.* **27,** 353–360 (2009).
37. Bern, M., Goldberg, D., McDonald, W. H. & Yates, J. R., III. Automatic quality assessment of peptide tandem mass spectra. *Bioinformatics* **20** (Suppl 1), i49–i54 (2004).
38. Eng, J., McCormack, A. & Yates, J. An approach to correlate tandem mass spectral data of peptides with amino acid sequences in a protein database. *J. Am. Soc. Mass Spectrom.* **5,** 976–989 (1994).
39. Peng, J., Elias, J. E., Thoreen, C. C., Licklider, L. J. & Gygi, S. P. Evaluation of multidimensional chromatography coupled with tandem mass spectrometry (LC/LC-MS/MS) for large-scale protein analysis: the yeast proteome. *J. Proteome Res.* **2,** 43–50 (2003).
40. Sadygov, R. G. *et al.* Code developments to improve the efficiency of automated MS/MS spectra interpretation. *J. Proteome Res.* **1,** 211–215 (2002).
41. Debacq-Chainiaux, F., Erusalimsky, J. D., Campisi, J. & Toussaint, O. Protocols to detect senescence-associated beta-galactosidase (SA-βgal) activity, a biomarker of senescent cells in culture and *in vivo*. *Nature Protocols* **4,** 1798–1806 (2009).